Inorganic Chemistry

pubs.acs.org/IC
Article

Synthesis of Na_3WH_9 and Na_3ReH_8 Ternary Hydrides at High Pressures

Tomas Marqueño, Israel Osmond, Mikhail A. Kuzovnikov, Hannah A. Shuttleworth, Samuel Gallego-Parra, Eugene Gregoryanz, Andreas Hermann, Ross T. Howie, and Miriam Peña-Alvarez*

Cite This: *Inorg. Chem.* 2024, 63, 21734−21741

Read Online

ACCESS | Metrics & More | Article Recommendations | Supporting Information

ABSTRACT: The Na−W−H and Na−Re−H ternary systems were studied in a diamond anvil cell through X-ray diffraction and Raman spectroscopy, supported by density functional theory and molecular dynamics calculations. Na_3WH_9 can be synthesized above 7.8 GPa and 1400 K, remaining stable between at least 0.1 and 42.1 GPa. The rhenium analogue Na_3ReH_8 can form at 10.1 GPa upon laser heating, being stable between at least 0.3 and 32.5 GPa. Na_3WH_9 and Na_3ReH_8 host $[WH_9]^{3-}$ and $[ReH_8]^{3-}$ anions, respectively, forming homoleptic 18-electron complexes in both cases. Both ternary hydrides show similar structural types and pressure dependent phase transitions. At the highest pressures they adopt a distorted fcc Heusler structure (Na_3WH_9−II′ and Na_3ReH_8−II′) while upon decompression the structure symmetrizes becoming fcc between ∼6.4 and 10 GPa for Na_3WH_9−II and at 17 GPa for Na_3ReH_8−II. On further pressure release, the fcc phases transform into variants of a (quasi-) hexagonal structure at ∼3 GPa, Na_3WH_9−I and Na_3ReH_8−I.

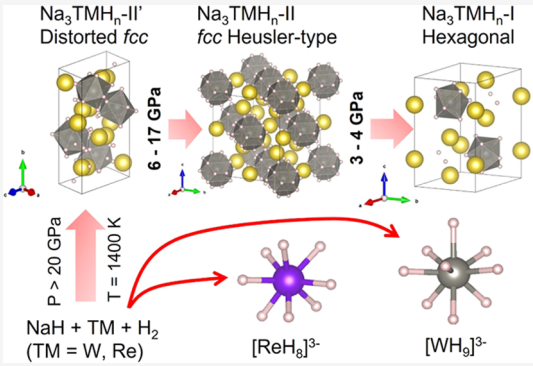

INTRODUCTION

The search for novel high-temperature superconductors has motivated the study of hydrogen-rich systems under high pressures, leading to the discovery of new binary metal−hydrogen compounds.[1] Some of these novel materials, such as LaH_{10},[2] CaH_6[3,4] or H_3S[5,6] exhibit superconducting properties with high critical temperature (T_c) above 150 GPa. Despite their promising attributes, such binary hydrides tend to decompose upon decompression, complicating the attainment of superconductive phases under ambient conditions.[7−9]

The study of ternary hydrides at high pressures has been suggested as an alternative approach toward achieving superconductivity at lower pressures.[10−12] This is because, the addition of a third element is expected to stabilize superconducting phases at lower pressures.[10,12−15] In fact, theoretical studies have predicted superconducting properties in compounds combining alkaline/alkaline earth metals with transition metal (TM) and hydrogen (complex transition metal hydrides, (CTMHs)), such as K_2ReH_9 (T_c = 127.1 K at 75 GPa)[16] or Mg_2IrH_6 (T_c = 160 K at ambient pressure).[10] However, experimental research has shown modest T_c values for CTMHs such as $BaReH_9$[17] and Li_5MoH_{11}[18] (above 100 GPa and below 10 K).

In CTMHs the TM atoms are coordinated by an unusually high number of hydrogen atoms forming homoleptic complex ions, such as $[OsH_7]^{3-}$,[19] $[NbH_9]^{4-}$,[20] and $[NiH_5]^{3-}$.[21] Traditionally, the synthesis of CTMHs has been conducted using autoclave techniques, where a mixture of active (alkali, alkaline earth or rare earth) and transition metals react at room pressure in a hydrogen atmosphere at high temperatures (300−700 °C).[13,22]

Historically, TMs from groups 3 to 6 were thought incapable of forming semiconducting CTMHs.[23] However, it was later shown that the use of large volume presses to 5 GPa and from 300 to 800 °C with AlH_3 as hydrogen precursor, leads to the synthesis of compounds such as Mg_3CrH_8,[24] $Li_5(TM)H_{11}$ (TM = Mo, W) and $Li_6(TM)H_{11}$ (TM = Nb, Ta).[20] All these compounds contain interstitial H^- anions as well as TMH_n homoleptic ionic complexes.

TM−H hydrides containing Na cations support high-coordinated TM complexes without interstitial H^-.[14,21] For TMs in groups 8, 9, and 10 these hydrides display a rich polymorphism in phases recovered to ambient conditions, with a *Pnma* structure type for Na_3NiH_5[21] and $Na_3(TM)H_6$ (TM = Co, Rh, Ir)[25] and a $P4_2/mnm$ structure type for $Na_3(TM)H_7$ (TM = Fe, Ru, Os).[14] In these CTMHs the hydrogen content decreases with the TM group number; therefore, Na−TM−H

Received: June 28, 2024
Revised: October 14, 2024
Accepted: October 17, 2024
Published: October 31, 2024

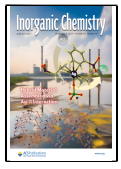

https://doi.org/10.1021/acs.inorgchem.4c02691
Inorg. Chem. 2024, 63, 21734−21741

with TMs from groups 6 and 7 could yield higher hydrogen-to-metal ratios (H to M ratio), which is beneficial for potential hydrogen storage applications. Under pressure, the Na-based CTMHs take up fcc-like structures with the metal atoms on Heusler sites, and rotationally disordered TMH_n complexes.

In this study, the synthesis of two novel Na−Re−H and Na−W−H compounds under high temperatures and pressures, using diamond anvil cells and infrared laser heating, are reported. Na_3WH_9 and Na_3ReH_8 form from NaH, W/Re and H_2 upon laser heating above 7.8 and 10.1 GPa, respectively, remaining stable between at least 30 GPa and down to <0.5 GPa. X-ray diffraction (XRD) and Raman spectroscopy, supported by density functional theory (DFT) calculations are used for the characterization of the new compounds. XRD measurements show that Na_3WH_9−II′ adopts a distorted fcc Heusler structure[26] above 20 GPa (the first identified rotationally ordered phase), containing $[WH_9]^{3-}$ units. Upon decompression, below 10 GPa, Na_3WH_9−II′ symmetrizes into an fcc structure (Na_3WH_9−II), which then transitions into an hexagonal structure, Na_3WH_9−I near ∼3 GPa.[26] Na_3ReH_8, which also adopts a Heusler structure with a small distortion, was synthesized from NaH + Re + H_2 at 32.5 and 25.5 GPa using laser heating to 1400 K. Na_3ReH_8 features stable 18-electron $[ReH_8]^{3-}$ complexes. Upon decompression, XRD measurements show that Na_3ReH_8 also undergoes a series of analogous phase transitions at 17 and 3.5 GPa. The Raman spectra of these phases present broad bands near 1100 and 2000 cm^{-1}, associated with TM−H bending and stretching modes of the $[TMH_n]^{-3}$ units, respectively. DFT ab initio calculations were used to evaluate the relative stability of the different structural phases for both ternary hydrides, reproducing the experimentally observed phase transitions. Additionally, molecular dynamics (MD) calculations captured the pseudorotational character of the Na_3WH_9−II and Na_3ReH_8−II structures, with hydrogen atoms occupying nonisotropic shells around the TM.

■ RESULTS

Powder X-ray Diffraction Experiments. Approximately two parts sodium hydride (NaH) to one part tungsten (W) by volume were loaded in a diamond anvil cell (DAC) and clamped with excess hydrogen (H_2) at 0.2 GPa. As shown in Figures 1(a,b) and S1−S3 the XRD patterns of the mixture fully transform during laser heating at 23.5 and 20 GPa (to 1400 K[27]). The new diffraction patterns are compatible with a distorted fcc Heusler arrangement,[26] with the Na and W atoms forming a metallic sublattice that can be described by either the space group *Immm* or *Pmnm* (Figure S2(a,b), respectively) in a proportion of 3:1 (Na_3WH_n). These are the highest symmetry subgroups of the fcc structure that are consistent with the experimental data presented here. Nevertheless, the stability of these structures is compromised when hydrogen atoms are incorporated into the DFT calculations. We performed DFT-based search for a possible arrangement of hydrogen atoms in this material, and found a possible candidate with the composition of Na_3WH_9 with a monoclinic crystal structure and space group $P2_1/c$. Rietveld refinements (Figure 1 (b)) of the crystal structure of the sample after laser heating at 23.5 GPa corroborate that this Na_3WH_9−II′ phase can be indexed to the monoclinic ($P2_1/c$) structure (a = 4.951 Å, b = 10.488(3) Å, c = 8.570(2) Å and β = 54.4(3) °C; R_{wp} = 32.5%). We will refer to this distorted cubic phase as Na_3WH_9−II′. Similarly, when the NaH−W−H_2 sample is compressed to 33.5 GPa and laser heated to 1400 K, Na_3WH_9−II′ is also formed (Figure S4(a,b)).

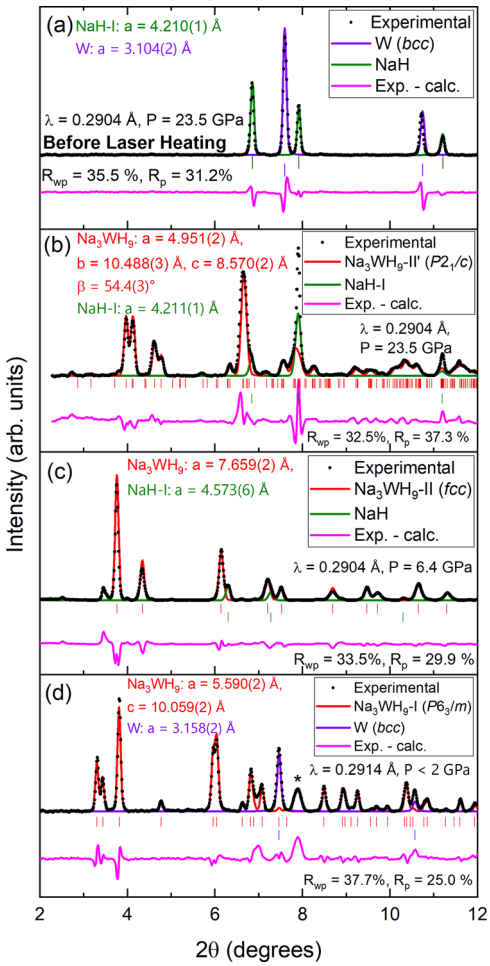

Figure 1. Rietveld refinements of powder XRD patterns at different pressures in two different experiments (λ = 0.2904 and 0.2914 Å). (a, b) Show the sample before and after laser heating, respectively. (c, d) Correspond to different phases observed upon decompression. The reflection labeled with an asterisk is associated with the rhenium gasket. Experimental data is depicted with black dots. The difference between the experimental and calculated pattern is depicted with a pink line. The calculated pattern for each individual phase is represented with its corresponding colored line, which is indicated on the legend. the March−Dollase model was used to account for preferred orientations. Pressures and both R_{wp} and R_p factors are shown on each plot. The calculated positions for the Bragg reflections of each phase are depicted with vertical ticks. The refined parameters for the Na_3WH_9 phases shown in (b−d) are shown in Tables S1−S3, respectively.

Upon compression up to 42 GPa, Na_3WH_9−II′ remains stable and no features of other Na−W−H phases are observed (Figure S5(c)).

Upon decompression of Na_3WH_9−II′, we observe the merging of some of its Bragg reflections at 6.4 GPa (Figures 1(c) and S1 and S5), indicating that the structure undergoes a phase transition to fcc Na_3WH_9−II, a more symmetric structure. At 5.5 GPa the XRD patterns are dominated by Na_3WH_9−II. When Na_3WH_9−II is further decompressed to 3 GPa, it undergoes a phase transition to Na_3WH_9−I, adopting a hexagonal structure (Figure 1(d)).[26] The patterns of Na_3WH_9−I can be indexed to a 3Na:W metallic sublattice with space groups $P6_3/mmc$[26] or $P6_3/cm$,[28] similar to those reported for Na_3As at low pressures. After considering hydrogen occupancies, DFT calculations reduce the total symmetry of the crystal to $P6_3/m$. A Rietveld refinement using a structure with

https://doi.org/10.1021/acs.inorgchem.4c02691
Inorg. Chem. 2024, 63, 21734−21741

space group $P6_3/m$ shows good compatibility with the experimental data (a = 5.590(2), c = 10.059(2) Å; R_{wp} = 37.7%), Figure 1 (d). All the phases found for Na_3WH_9−II′ (42−6.4 GPa), -II (6.4−3 GPa) and -I (below 3 GPa) are characterized by $[WH_9]^{3-}$ anionic units. These accommodate 18 valence electrons, with tungsten achieving its highest (and most common) oxidation state (+6).

In a different set of experiments, we loaded NaH, Re and H_2 gas at 0.2 GPa in a DAC. The sample was compressed to 32.5 GPa and laser-heated using the rhenium metal as a coupler. XRD patterns of the sample before and after heating are shown in Figure 2(a,b). As in Na_3WH_9−II′, the diffraction peak distribution of the product, Na_3ReH_8−II′, resembles those of an fcc lattice, the Bragg peaks of the phase synthesized after laser heating at 32.5 GPa are not symmetric and can be more accurately described by an orthorhombic distortion of the structure. In fact, our DFT calculations reduce the fcc Heusler of Na_3ReH_8 to a slightly distorted variant, which shows a reasonably good compatibility with our data, as shown in the Rietveld refinement depicted in Figure 2 (b) ($Pca2_1$; a = 9.711(1) Å, b = 6.898(1) Å and c = 9.607(2) Å; R_{wp} = 33.3%). We suggest the formula Na_3ReH_8, as only in the $[ReH_8]^{3-}$ ions can accommodate 18 valence electrons. Hence, whereas W is in its highest oxidation state +6, Re can only achieve its +5 oxidation state in Na−TM−H compounds.

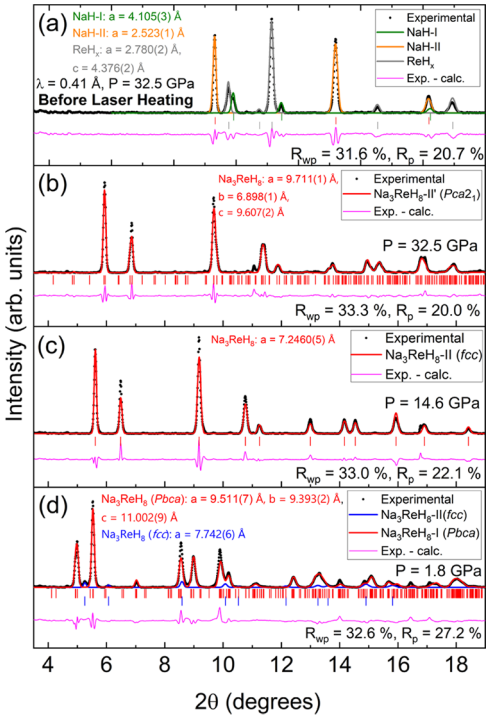

Figure 2. XRD patterns and corresponding Rietveld refinements of the Na−Re−H sample before laser heating (a), after laser heating (b) and subsequently decompressed down to 14.6 (c) and 1.8 GPa (d). Experimental data is represented with black dots. The difference between these and the refinement is depicted with a pink solid line. The rest of the colored solid lines correspond to the calculated partial contributions the phases indicated on the legends. Vertical ticks denote the position of the Bragg reflections. The refined parameters for the Na_3ReH_8 phases shown in (b−d) are presented in Tables S4−S6, respectively.

As in Na_3WH_9, Na_3ReH_8−II′ transitions to fcc Na_3ReH_8−II (Figures 2(c) and S6(a,b): upon decompression at around 17 GPa, the (020) and (202) reflections of Na_3ReH_8−II′ merge into a single (200) reflection characteristic of an fcc phase). At 1.8 GPa, the XRD patterns of Na_3ReH_8 present a different peak distribution that corresponds to a new low-pressure phase Na_3ReH_8−I, Figure 2(d). Similarly to Na_3WH_9−I, we initially considered a highly symmetric hexagonal lattice for Na_3ReH_8−I, which our DFT calculations reduced to a $Pbca$ symmetry. Rietveld refinements in Figure 2(d) show a reasonably good compatibility with this structural model (a = 9.511(7) Å, b = 9.393(2) Å, c = 11.002(9) Å; R_{wp} = 32.6%). In this structure, the Re atoms lay on a quasi-hexagonal sublattice, similar to that of Na_3WH_9−I. Laser heating the reactants at 25.5 GPa yields identical products and phase transformations under decompression (see Figure S6(c)).

Figure 3(a,b) present lattice parameters and unit-cell volumes per formula unit as a function of pressure for the Na_3WH_9 and Na_3ReH_8 phases. The unit-cell volumes are compared with the sum of the individual volumes of the reactants, considering different hydrogen amounts.[29−32] In all cases, the experimental volumes for both Na−W−H and Na−Re−H compounds are smaller than the sums of the individual volumes of the reagents i.e., all the suggested stoichiometries fulfill Le Châtelier's principle regarding volume change upon reaction. Despite hydrogen disorder is expected in the fcc phases, the lattice parameters of the H-ordered phases are in reasonably good agreement with the experimental results (Figure 3). The subgroup axis transformation relating the $P2_1/c$ space group to the Heusler structure is $(a, b, c \sin\beta) = (a_{fcc}/\sqrt{2}, a_{fcc}\sqrt{2}, a_{fcc})$. For $Pca2_1$, this relationship is $(a, b, c) = (a_{fcc}\sqrt{2}, a_{fcc}, a_{fcc}\sqrt{2})$. Random preferred orientations in our patterns lead to some deviations between the refined (Tables S1−S11) and DFT calculated (Tables S12−S15) atomic coordinates at similar pressures.

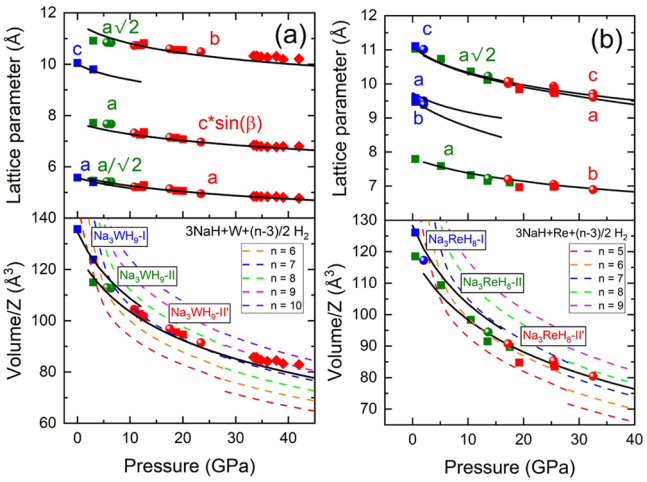

Figure 3. Pressure dependence of the lattice parameters and volumes per formula unit of (a) Na_3WH_9 and (b) Na_3ReH_8. Circles, squares and diamonds correspond to the data collected during different sets of experiments. The II′, II, and I phases are indicated with red, green and blue symbols, respectively. Our calculated DFT values are depicted with black solid lines. Colored dashed lines correspond to the sum of the reactant volumes (NaH, TM, H_2)[29−32] for different quantities of hydrogen (values of n). The discontinuity in these lines correspond to the NaH-I to NaH-II phase transition at ∼29 GPa.[29]

Figure 4 shows $\Delta H(P)$, the relative enthalpy curves between 0 and 40 GPa for the Na−W−H and Na−Re−H systems calculated with DFT. The formation enthalpies of the reaction

https://doi.org/10.1021/acs.inorgchem.4c02691
Inorg. Chem. 2024, 63, 21734−21741

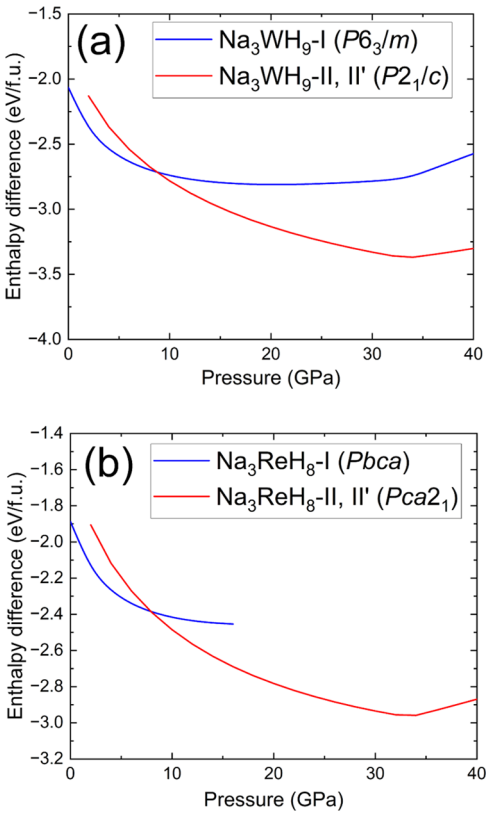

Figure 4. ΔH vs P curves of the (a) Na−W−H and (b) Na−Re−H systems. The color corresponding to each phase is indicated in the legend. The difference in enthalpy was calculated with respect to the enthalpy of the separate reactants i.e., H(NaH) + H(TM) + $H(H_2)$. Enthalpy units are given in eV per formula unit (f.u.).

products were calculated with respect to the sum of the enthalpies of NaH, TM (W, Re) and H_2. The dynamic stability of the II′ and I phases of Na_3WH_9 and Na_3ReH_8 was confirmed by DFT (see calculated phonon bands in Figure S7). The fcc structures Na_3WH_9−II and Na_3ReH_8−II can only be stabilized dynamically, i.e., through MD simulations, therefore DFT calculations at T = 0 K reduce the Heusler fcc structure to the $P2_1/c$ ($Pca2_1$) symmetry. For the Na−W−H system, Na_3WH_9 is predicted to have lower enthalpy than its separate reactants across the considered pressure range (P < 40 GPa). Below 8 GPa, the hexagonal Na_3WH_9−I ($P6_3/m$) phase becomes more stable than the Na_3WH_9−II′ (distorted cubic $P2_1/c$) phase, in good agreement with the experimental transition between 5.5 and 3 GPa during decompression. In the Na−Re−H system, (Figure 4(b)) both Na_3ReH_8−I ($Pbca$) and Na_3ReH_8−II′ ($Pca2_1$) show negative values of ΔH in the 0 to 40 GPa range. DFT predicts the transition from the high- to the low-pressure phase below 9 GPa, supporting our experimental observations. Interestingly, Na_3WH_9−I and Na_3ReH_8−I both exhibit negative values of ΔH at low pressures, indicating their stability at ambient conditions. However, relative Gibbs free energies ΔG (not calculated here), particularly when considering hydrogen, might favor their decomposition. Unfortunately, the product reacts with the moisture in the air when the DAC is opened, so its stability at ambient conditions was not explored.

The DFT calculated crystal structures of the high pressure phases, Na_3WH_9−II′ ($P2_1/c$) and Na_3ReH_8−II′ ($Pca2_1$), (assuming static positions for hydrogen atoms i.e., full occupancies) is depicted in Figure 5(a,b), respectively. Na_3WH_9−II′ consists of an arrangement of Na^+ cations and $[WH_9]^{3-}$ anionic units, in which the Na and W atoms form a slightly distorted Heusler fcc structure. Crystallographic data for the high-pressure phases Na_3WH_9−II′ and Na_3ReH_8−II′ obtained from DFT calculations are given in Tables S12 and S13, respectively.

Figure 5(c) shows the unit-cell corresponding to the Na_3WH_9−II structure (fcc) obtained after MD calculations in which H atoms have 1/2 partial occupations. This Heusler arrangement (fcc) has been reported for Na_3FeH_7, Na_3CoH_6, Na_3NiH_5 and K_3ReH_6.[14,21,33] As shown in Figure S8(a), hydrogen atoms are delocalized around the transition metal atoms, occupying spherical shells due to rotation of the $[WH_9]^{3-}$ anions. The anion complex' rotations are not fully free, and hydrogen angular distribution is uneven. The calculated time

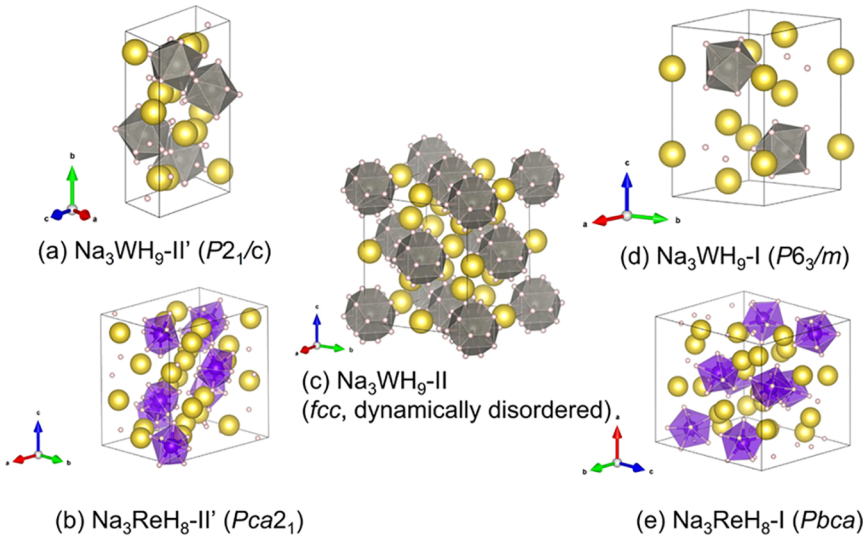

Figure 5. Crystal structures of Na_3WH_9 and Na_3ReH_8 obtained in calculations: (a) Na_3WH_9−II′ ($P2_1/c$, DFT), (b) Na_3ReH_8 ($Pca2_1$, DFT), (c) Na_3WH_9−II (fcc, MD), (d) Na_3WH_9−I ($P6_3/m$, DFT) and (e) Na_3ReH_8−I ($Pbca$, DFT). Yellow, gray, purple and white spheres represent Na, W, Re, and H atoms, respectively. Gray and purple polyhedra represent $[WH_9]^{3-}$ and $[ReH_8]^{3-}$.

https://doi.org/10.1021/acs.inorgchem.4c02691
Inorg. Chem. 2024, 63, 21734−21741

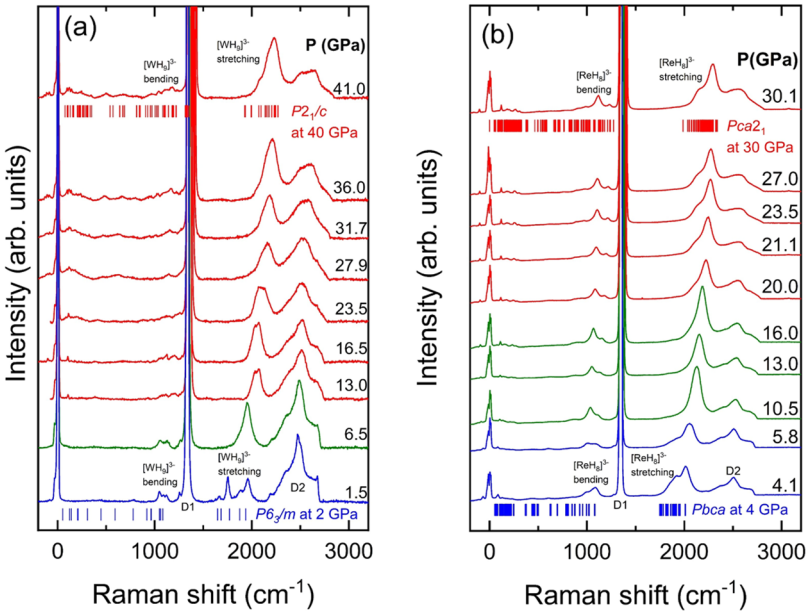

Figure 6. Raman spectra of the (a) Na_3WH_9 (decompression) and (b) Na_3ReH_8 (compression) phases. The spectra corresponding to the II′, II, and I phases are depicted with red, green and blue lines, respectively. The bands indicated with the labels "D1" and "D2" correspond to the first and second Raman modes of diamond. Vertical ticks stand for the calculated frequencies of the phases indicated in the figure.

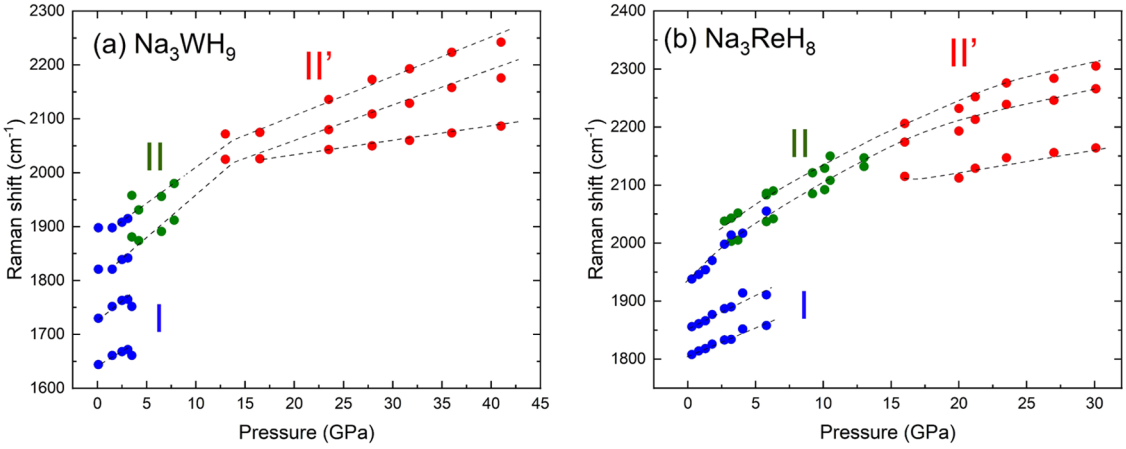

Figure 7. Pressure dependence of the individual Raman bands composing the $[TMH_n]^{3-}$ stretching modes of (a) Na_3WH_9 and (b) Na_3ReH_8. Dashed lines are a guide to the eye.

evolution of the lattice parameters for this phase is depicted in Figure S8(b,c), showing how the structure reduces into an fcc lattice with time. Our MD calculations show the equivalent time evolution of the lattice parameters of Na_3ReH_8−II at 0, 4, 10, and 20 GPa in Figure S9. These results indicate that pressure reduces hydrogen mobility, hindering rotational degrees of freedom, eventually causing the transition from the rotationally disordered fcc (II) to the distorted high-pressure phases (II′) in both Na_3WH_9 and Na_3ReH_8.

The Na_3WH_9−I phase ($P6_3/m$) shown in Figure 5(d) can be described as an arrangement of two types of linear structures disposed along the *c*-axis direction: pure Na chains and (−Na−Na−$[WH_9]^{3-}$)− chains. The WH_9 complexes form a hexagonal close packed structure, with the Na atoms from the pure Na chains occupying centers of the in-planar triangles located in between the two octa-sites; and the remaining Na atoms occupying tetrahedral interstitial sites. The Na_3ReH_8−I phase (*Pbca*), whose unit-cell is depicted in Figure 5(e), can be seen as a 4-fold supercell of the hexagonal structure, for instance as (a_o, b_o, c_o) = ($a_h + 2b_h$, c_h, $2a_h$). DFT calculated crystallographic data for the two phases is given in Tables S14 and S15. The symmetry-lowering in Na_3ReH_8−I manifests in the metal lattice as in-plane displacement of the tetrahedral site Na atoms. We performed DFT-MD simulations of Na_3ReH_8−I at 2 GPa and noticed that this displacement disappeared upon heating when (simultaneously) the $[ReH_8]^{3-}$ units became rotationally disordered (Figure S10). Hence, we expect that at low pressure but high temperature, Na_3ReH_8 also takes up a hexagonal phase; at low temperature, a disorder−order transition occurs as the $[ReH_8]^{3-}$ complex is not compatible with hexagonal symmetry.

Raman Spectroscopy Experiments. As illustrated in Figures 6(a) and S11(a), the Raman spectra of Na_3WH_9−II′ exhibit prominent bands in the 1000−1300 and 1900−2500 cm^{-1} ranges, which correspond to the bending and stretching modes of the $[TMH_n]^{3-}$ anionic units.[17,20,34−36] Particular attention is given to the 1900−2500 cm^{-1} region, indicative of the TM−H stretching mode. Density functional theory (DFT) predicts that the Raman spectra are composed of numerous

https://doi.org/10.1021/acs.inorgchem.4c02691
Inorg. Chem. 2024, 63, 21734−21741

closely spaced contributions. By analyzing the second derivative of the experimentally obtained spectra at 41 GPa, we identified three distinct components for Na_3WH_9−II′ (see Figure S12(a)). Upon decompression from 16.5 to 6.5 GPa, significant spectral changes are observed in the TM−H stretching modes, transitioning from three distinct components to one intense peak with a low-frequency shoulder. This is related with the Na_3WH_9−II′ to Na_3WH_9−II phase transition. Further decompression to 3.5 GPa results in an additional splitting of these TM−H stretching modes into five components, Figure S12(c), which is attributed to the transition to the Na_3WH_9−I phase, which aligns well with the DFT-predicted modes illustrated in Figure 6(a).

Analogous to the Na−W−H system, the Raman spectra of Na_3ReH_8−II′ exhibit two principal Raman active regions around 1100 and 2100 cm^{-1}, corresponding to the transition metal−hydrogen (TM−H) bending and stretching modes, respectively (Figures S11(b) and 6(b)). Similar to Na_3WH_9−II′, the Raman spectra of Na_3ReH_8−II′ at approximately 30 GPa in the TM−H stretching region are characterized by multiple contributions predicted by DFT. Through second derivative analysis of the experimental spectrum, we resolved three contributions (Figure S12(d)). Additionally, between 20 and 16 GPa, coinciding with the phase transition to Na_3ReH_8−II, the spectra simplify, particularly in the TM−H modes region, which reduce from three to two contributions (Figure S12(e)). During compression from 5.8 to 10.5 GPa (Figure 6(b)) and decompression from 3.7 to 3.2 GPa (Figure S12(b)), coinciding with the phase transition to Na_3ReH_8−I, the spectra undergo notable changes. These changes are especially relevant in the TM−H stretching region, which becomes more complex with over ten contributions predicted by DFT, experimentally resolved as three (Figure S12(f)).

The pressure evolution of the TM−H stretching modes contributions is depicted in Figure 7(a),(b) for Na_3WH_9 and Na_3ReH_8, respectively. There is no significant effect of the transition metal (TM) on the Raman shift of the TM−H stretching modes, as both Re and W are located in the same spectral region. Consistent with other ternary transition metal polyhydrides, regardless of the phase, all spectral contributions in both Na_3WH_9 and Na_3ReH_8 upshift with pressure, which is related to the shortening of the TM−H bond under pressure.[12,20] The lower frequency of the TM−H stretching modes associated with the low-pressure hexagonal phases, Na_3WH_9−I and Na_3ReH_8−I, is related to a decrease in the electronic density of the TM−H bond, leading to an expansion of the $[TMH_n]^{3-}$ unit. A similar analysis was carried out for the H−TM−H bending modes of Na_3WH_9 and Na_3ReH_8, shown in Figure S13(a,b), respectively.

To explore the stability of Na_3WH_9, a NaH−W−H_2 sample was laser heated at different pressures. Laser heating at 1 GPa and 1400 K did not lead to any spectral changes, indicating no reaction between the precursors. However, laser heating to approximately 1400 K at 7.8 GPa induced spectral changes related to the formation of Na_3WH_9−II, as shown in Figure S14(a). Analogous experiments were conducted for the NaH−Re−H_2 system. Laser heating at 1 GPa and 1400 K did not result in the formation of Na_3ReH_8. It was only at pressures above 10 GPa and temperatures of 1400 K that the spectral features of Na_3ReH_8−II were identifiable upon quenching, Figure S14(b).

Discussion. The synthesis of Na_3WH_9 and Na_3ReH_8 demonstrates the feasibility of forming Na−TM−H compounds with TM of groups 6 and 7 using high pressures and laser heating techniques. Stable novel Na−TM−H compounds featuring d^0 $[WH_9]^{3-}$ and d^2 $[ReH_8]^{3-}$ homoleptic anions are proven. These anionic units accommodate 18 valence electrons and may be common to other Na−TM−H compounds with TMs of groups 6 and 7. $[ReH_8]^{3-}$ represents an interesting case, as this coordination is highly unusual in CTMHs, in which the highest coordination of TM elements is usually either 7 or 9.[13] In fact, only few systems are known to host 8-coordinated TM atoms, such as Cs_3OsH_9 and Rb_3OsH_9.[19,37,38] Other systems with similar stoichiometries to Na_3ReH_8, such as Mg_3CrH_8 host $[CrH_7]^{5-}$ anions and interstitial H^-.[24,25]

As mentioned in Na_3WH_9−II and Na_3ReH_8−II, the $[WH_9]^{3-}$ and $[ReH_8]^{3-}$ anions are in freely rotating states. Low temperatures and high pressures can induce similar distortions, as both restrict dynamic effects. For instance, it has been observed that in Na_3NiH_5 the fcc structure observed at 5 GPa and 700 K becomes a quasi-cubic orthorhombic structure when quenched at room temperature. Likewise, reversible transitions from rotational to nonrotational states are the foundation of thermal energy storage in solid−solid phase change materials (ss-PCM's),[39,40] which in some cases exhibit crystallographic transformations similar to those seen in the hydride systems in this study.[41]

Both, Na_3WH_9 and Na_3ReH_8 remain transparent within the whole experimental pressure range. To check for possible metallic phases, we calculated the pressure evolution of the electronic band gap of Na_3WH_9−II′ and Na_3ReH_8−II′, (Figure S15). The band gap of Na_3WH_9−II′ ($P2_1/c$) is predicted to progressively close with increasing pressure, becoming metallic above 180 GPa. Na_3ReH_8−II′ is expected to have a smaller band gap than Na_3WH_9−II′ below 100 GPa, but it would only decrease substantially above 350 GPa, suggesting that metallicity can only be achieved at extremely high pressures (over 500 GPa). The main reason for the lack of metallicity at more attainable pressures is that $[TMH_x]^{3-}$ anions are disconnected and considerably separated from each other inside the reported structures, which prevents the formation of a monatomic hydrogen framework.[2]

■ CONCLUSIONS

By combining both XRD and Raman scattering techniques we explore the Na−W(Re)−H ternary systems under pressure. We observed the formation of distinct high-hydrogen content structures that we investigated upon decompression. Na_3WH_9 can be synthesized above 7.8 GPa after laser heating, featuring 18-electron $[WH_9]^{3-}$ homoleptic units. In the Na−Re−H system, Na_3ReH_8 was synthesized at 32.5 and 10.1 GPa, with $[ReH_8]^{3-}$ units. Upon decompression from about 40 GPa, these structures undergo analogous phase transitions: II′(distorted fcc) → II (Heusler fcc)→ I (distorted hcp). The specific distortion scenarios and transition pressures depend on the transition metal. Experiments and theoretical calculations indicate that these ternary compounds are stable to pressures below 1 GPa, making them good candidates for hydrogen storage materials, however, Na_3WH_9 and Na_3ReH_8 are electrical insulators with wide bandgaps. The thermodynamic stability of the different observed polymorphs was studied via DFT and MD calculations, showing excellent compatibility with the experimentally reported structural transformations.

https://doi.org/10.1021/acs.inorgchem.4c02691
Inorg. Chem. 2024, 63, 21734−21741

■ ASSOCIATED CONTENT

Supporting Information

The Supporting Information is available free of charge at https://pubs.acs.org/doi/10.1021/acs.inorgchem.4c02691.

Description of the experimental and computational details, (ii) additional XRD and Raman data from different samples, (iii) results on MD calculations, (iv) calculated pressure evolution of the band gap of Na_3WH_9 and (v) DFT calculated atomic positions for different phases (PDF)

Accession Codes

Deposition Numbers 2367343−2367344 and 2383663−2383664 contain the supplementary crystallographic data for this paper. These data can be obtained free of charge via the joint Cambridge Crystallographic Data Centre (CCDC) and Fachinformationszentrum Karlsruhe Access Structures service.

■ AUTHOR INFORMATION

Corresponding Author

Miriam Peña-Alvarez − *Center for Science at Extreme Conditions (CSEC) and the School of Physics and Astronomy, The University of Edinburgh, Edinburgh EH3 9FD, U.K.;* orcid.org/0000-0001-7056-7158; Email: miriam.pena.alvarez@ed.ac.uk

Authors

Tomas Marqueño − *Center for Science at Extreme Conditions (CSEC) and the School of Physics and Astronomy, The University of Edinburgh, Edinburgh EH3 9FD, U.K.;* orcid.org/0000-0001-5371-1082

Israel Osmond − *Center for Science at Extreme Conditions (CSEC) and the School of Physics and Astronomy, The University of Edinburgh, Edinburgh EH3 9FD, U.K.;* orcid.org/0000-0001-8756-8501

Mikhail A. Kuzovnikov − *Center for Science at Extreme Conditions (CSEC) and the School of Physics and Astronomy, The University of Edinburgh, Edinburgh EH3 9FD, U.K.;* orcid.org/0000-0003-4030-4861

Hannah A. Shuttleworth − *Center for Science at Extreme Conditions (CSEC) and the School of Physics and Astronomy, The University of Edinburgh, Edinburgh EH3 9FD, U.K.;* orcid.org/0000-0002-5113-1575

Samuel Gallego-Parra − *European Synchrotron Radiation Facility (ESRF), Grenoble 38000, France*

Eugene Gregoryanz − *Center for Science at Extreme Conditions (CSEC) and the School of Physics and Astronomy, The University of Edinburgh, Edinburgh EH3 9FD, U.K.; Key Laboratory of Materials Physics, Institute of Solid State Physics, HFIPS, Chinese Academy of Sciences, Hefei 230031, China; Center for High Pressure Science and Technology Advanced Research (HPSTAR), Shanghai 201203, China*

Andreas Hermann − *Center for Science at Extreme Conditions (CSEC) and the School of Physics and Astronomy, The University of Edinburgh, Edinburgh EH3 9FD, U.K.;* orcid.org/0000-0002-8971-3933

Ross T. Howie − *Center for Science at Extreme Conditions (CSEC) and the School of Physics and Astronomy, The University of Edinburgh, Edinburgh EH3 9FD, U.K.; Center for High Pressure Science and Technology Advanced Research (HPSTAR), Shanghai 201203, China;* orcid.org/0000-0002-7013-8211

Complete contact information is available at: https://pubs.acs.org/10.1021/acs.inorgchem.4c02691

Notes

The authors declare no competing financial interest.

■ ACKNOWLEDGMENTS

The work was supported by the UKRI Future Leaders fellowship Mrc-Mr/T043733/1 and by the European Research Council (ERC) under the European Union's Horizon 2020 research and innovation programme (Grant agreement no. 948895, MetElOne). The authors thank Prof. M. McMahon for allowing us to use the glovebox of his laboratory to load the samples. We acknowledge DESY (Hamburg, Germany), a member of the Helmholtz Association HGF, for the provision of beamline P02.2 at PETRA-III, allocated under proposals I-20220830, I-20221042, I-20221366 and I-20230232. We would like to thank beamline scientists Nico Giordano, Konstantin Glazyrin and Hanns-Peter Lierman for their help during the experiments. The ESRF (Grenoble, France) is acknowledged for providing access to beamline ID15B for the experiment HC-5457. We would like to thank beamline scientists Michael Hanfland, Gaston Garbarino, Mohamed Mezouar and Samuel Gallego-Parra. Computational resources provided by the UK's National Supercomputer Service through the UK Car−Parrinello HEC consortium (EP/X035891/1) and by the UK Materials and Molecular Modelling Hub (EP/P020194) are gratefully acknowledged.

■ REFERENCES

(1) Sun, Y.; Zhong, X.; Liu, H.; Ma, Y. Clathrate metal superhydrides under high-pressure conditions: enroute to room-temperature superconductivity. *Natl. Sci. Rev.* **2024**, *11*, No. nwad270, DOI: 10.1093/nsr/nwad270.

(2) Drozdov, A. P.; Kong, P.; Minkov, V.; Besedin, S.; Kuzovnikov, M.; Mozaffari, S.; Balicas, L.; Balakirev, F.; Graf, D.; Prakapenka, V.; et al. Superconductivity at 250 K in lanthanum hydride under high pressures. *Nature* **2019**, *569*, 528−531.

(3) Li, Z.; He, X.; Zhang, C.; Wang, X.; Zhang, S.; Jia, Y.; Feng, S.; Lu, K.; Zhao, J.; Zhang, J.; et al. Superconductivity above 200 K discovered in superhydrides of calcium. *Nat. Commun.* **2022**, *13*, No. 2863.

(4) Ma, L.; Wang, K.; Xie, Y.; Yang, X.; Wang, Y.; Zhou, M.; Liu, H.; Yu, X.; Zhao, Y.; Wang, H.; et al. High-temperature superconducting phase in clathrate calcium hydride CaH 6 up to 215 K at a pressure of 172 GPa. *Phys. Rev. Lett.* **2022**, *128*, No. 167001.

(5) Drozdov, A.; Eremets, M.; Troyan, I.; Ksenofontov, V.; Shylin, S. I. Conventional superconductivity at 203 K at high pressures in the sulfur hydride system. *Nature* **2015**, *525*, 73−76.

(6) Osmond, I.; Moulding, O.; Cross, S.; Muramatsu, T.; Brooks, A.; Lord, O.; Fedotenko, T.; Buhot, J.; Friedemann, S. Clean-limit superconductivity in $Im\bar{3}m H_3S$ synthesized from sulfur and hydrogen donor ammonia borane. *Phys. Rev. B* **2022**, *105*, No. L220502.

(7) Kuzovnikov, M. A.; Tkacz, M. Synthesis of ruthenium hydride. *Phys. Rev. B* **2016**, *93*, No. 064103.

(8) Kuzovnikov, M. A.; Tkacz, M. High-pressure synthesis of novel polyhydrides of Zr and Hf with a Th_4H_{15}-type structure. *J. Phys. Chem. C* **2019**, *123*, 30059−30066.

(9) Marqueño, T.; Kuzovnikov, M. A.; Osmond, I.; Dalladay-Simpson, P.; Hermann, A.; Howie, R. T.; Peña-Alvarez, M. High pressure study of sodium trihydride. *Front. Chem.* **2023**, *11*, No. 1306495, DOI: 10.3389/fchem.2023.1306495.

(10) Dolui, K.; Conway, L. J.; Heil, C.; Strobel, T. A.; Prasankumar, R. P.; Pickard, C. J. Feasible route to high-temperature ambient-pressure hydride superconductivity. *Phys. Rev. Lett.* **2024**, *132*, No. 166001.

(11) Sun, W.; Chen, B.; Li, X.; Peng, F.; Hermann, A.; Lu, C. Ternary Na-P-H superconductor under high pressure. *Phys. Rev. B* **2023**, *107*, No. 214511.
(12) Hansen, M. F.; Conway, L. J.; Dolui, K.; Heil, C.; Pickard, C. J.; Pakhomova, A.; Mezouar, M.; Kunz, M.; Prasankumar, R. P.; Strobel, T. A. Synthesis of Mg_2IrH_5: A potential pathway to high-T_c hydride superconductivity at ambient pressure, arXiv:2406.09538. arXiv.org e-Print archive, 2024 https://arxiv.org/abs/2406.09538.
(13) Yvon, K.; Renaudin, G. Hydrides: solid state transition metal complexes. *Encycl. Inorg. Chem.* **2006**, *III*, 1814−1846.
(14) Spektor, K.; Crichton, W. A.; Filippov, S.; Simak, S. I.; Fischer, A.; Haussermann, U. Na_3FeH_7 and Na_3CoH_6: hydrogen-rich first-row transition metal hydrides from high pressure synthesis. *Inorg. Chem.* **2020**, *59*, 16467−16473.
(15) He, X.-l.; Zhao, W.; Xie, Y.; Hermann, A.; Hemley, R. J.; Liu, H.; Ma, Y. Predicted hot superconductivity in $LaSc_2H_{24}$ under pressure. *Proc. Natl. Acad. Sci. U.S.A.* **2024**, *121*, No. e2401840121.
(16) Zhao, Y.; Zhang, X.; Li, X.; Ding, S.; Liu, Y.; Yang, G. Emergent superconductivity in K 2 ReH 9 under pressure. *J. Mater. Chem. C* **2022**, *10*, 14626−14632.
(17) Muramatsu, T.; Wanene, W. K.; Somayazulu, M.; Vinitsky, E.; Chandra, D.; Strobel, T. A.; Struzhkin, V. V.; Hemley, R. J. Metallization and superconductivity in the hydrogen-rich ionic salt $BaReH_9$. *J. Phys. Chem. C* **2015**, *119*, 18007−18013.
(18) Meng, D.; Sakata, M.; Shimizu, K.; Iijima, Y.; Saitoh, H.; Sato, T.; Takagi, S.; Orimo, S.-i. Superconductivity of the hydrogen-rich metal hydride Li_5MoH_{11} under high pressure. *Phys. Rev. B* **2019**, *99*, No. 024508.
(19) Bronger, W.; Sommer, T.; Auffermann, G.; Müller, P. New alkali metal osmium-and ruthenium hydrides. *J. Alloys Compd.* **2002**, *330*−*332*, 536−542.
(20) Takagi, S.; Iijima, Y.; Sato, T.; Saitoh, H.; Ikeda, K.; Otomo, T.; Miwa, K.; Ikeshoji, T.; Orimo, S.-I. Formation of novel transition metal hydride complexes with ninefold hydrogen coordination. *Sci. Rep.* **2017**, *7*, No. 44253.
(21) Spektor, K.; Crichton, W. A.; Filippov, S.; Klarbring, J.; Simak, S. I.; Fischer, A.; Haussermann, U. Na−Ni−H phase formation at high pressures and high temperatures: hydrido complexes $[NiH_5]^{3-}$ versus the perovskite $NaNiH_3$. *ACS Omega* **2020**, *5*, 8730−8743.
(22) Bronger, W. Synthesis and structure of new metal hydrides. *J. Alloys Compd.* **1995**, *229*, 1−9.
(23) King, R. B. *Encyclopedia of Inorganic Chemistry*; Wiley Online Library, 2005; Vol. *10*.
(24) Takagi, S.; Iijima, Y.; Sato, T.; Saitoh, H.; Ikeda, K.; Otomo, T.; Miwa, K.; Ikeshoji, T.; Aoki, K.; Orimo, S.-I. True Boundary for the Formation of Homoleptic Transition-Metal Hydride Complexes. *Angew. Chem., Int. Ed.* **2015**, *54*, 5650−5653.
(25) Spektor, K.; Crichton, W. A.; Filippov, S.; Simak, S. I.; Haussermann, U. Exploring the Mg−Cr−H system at high pressure and temperature via in situ synchrotron diffraction. *Inorg. Chem.* **2019**, *58*, 11043−11050.
(26) Beister, H. J.; Syassen, K.; Klein, J. Phase transition of Na_3As under pressure. *Z. Naturforsch. B* **1990**, *45*, 1388−1392.
(27) Sapritsky, V. I. Black-body radiometry. *Metrologia* **1995**, *32*, No. 411.
(28) Hafner, P.; Range, K.-J. Na3As revisited: high-pressure synthesis of single crystals and structure refinement. *J. Alloys Compd.* **1994**, *216*, 7−10.
(29) Duclos, S. J.; Vohra, Y. K.; Ruoff, A. L.; Filipek, S.; Baranowski, B. High-pressure studies of NaH to 54 GPa. *Phys. Rev. B* **1987**, *36*, No. 7664.
(30) Dewaele, A.; Loubeyre, P.; Mezouar, M. Equations of state of six metals above 94 GPa. *Phys. Rev. B* **2004**, *70*, No. 094112.
(31) Anzellini, S.; Dewaele, A.; Occelli, F.; Loubeyre, P.; Mezouar, M. Equation of state of rhenium and application for ultra high pressure calibration. *J. Appl. Phys.* **2014**, *115*, No. 043511, DOI: 10.1063/1.4863300.
(32) Loubeyre, P.; LeToullec, R.; Hausermann, D.; Hanfland, M.; Hemley, R.; Mao, H.; Finger, L. X-ray diffraction and equation of state of hydrogen at megabar pressures. *Nature* **1996**, *383*, 702−704.
(33) Bronger, W.; Auffermann, G.; Schilder, H. K_3ReH_6−Synthese, Struktur und magnetische Eigenschaften. *Z. Anorg. Allg. Chem.* **1998**, *624*, 497−500.
(34) Barsan, M. M.; Moyer, R. O., Jr.; Butler, I. S.; Gilson, D. F. Pressure dependence of the Raman spectra of salts of hexahydridoruthenate (II), M_2RuH_6 (M= Ca, Sr, Eu) and their deuteride analogues. *J. Alloys Compd.* **2006**, *424*, 73−77.
(35) Marizy, A.; Geneste, G.; Garbarino, G.; Loubeyre, P. High pressure polymorphism of LiBH 4 and of NaBH 4. *RSC Adv.* **2021**, *11*, 25274−25283.
(36) Reed, D.; Book, D. Recent applications of Raman spectroscopy to the study of complex hydrides for hydrogen storage. *Curr. Opin. Solid State Mater. Sci.* **2011**, *15*, 62−72.
(37) Takagi, S.; Ikeshoji, T.; Sato, T.; Orimo, S.-i. Pseudorotating hydride complexes with high hydrogen coordination: A class of rotatable polyanions in solid matter. *Appl. Phys. Lett.* **2020**, *116*, No. 173901.
(38) Auffermann, G.; Bronger, W.; Müller, P.; Roth, G.; Schilder, H.; Sommer, T. Cs_3OsH_9-Synthese, Struktur und magnetische Eigenschaften. *Z. Anorg. Allg. Chem.* **2005**, *631*, 1060−1064.
(39) Fallahi, A.; Guldentops, G.; Tao, M.; Granados-Focil, S.; Van Dessel, S. Review on solid-solid phase change materials for thermal energy storage: Molecular structure and thermal properties. *Appl. Therm. Eng.* **2017**, *127*, 1427−1441.
(40) Bayon, A.; Liu, M.; Sergeev, D.; Grigore, M.; Bruno, F.; Müller, M. Novel solid−solid phase-change cascade systems for high-temperature thermal energy storage. *Sol. Energy* **2019**, *177*, 274−283.
(41) Konar, S.; Zieniute, G.; Lascelles, E.; Wild, B.; Hermann, A.; Wang, Y.; Quinn, R. J.; Bos, J.-W. G.; Fitch, A. Revisiting Solid−Solid Phase Transitions in Sodium and Potassium Tetrafluoroborate for Thermal Energy Storage. *Chem. Mater.* **2024**, *36*, 1238−1248.